JOURNAL OF EXPERIMENTAL AND THEORETICAL PHYSICS, 2024, Vol. 165, No. 5, pp. 707–716

ORDER, DISORDER, AND PHASE TRANSITION IN CONDENSED MEDIA

FEATURES OF ANISOTROPY IN NARROW STRIPS OF THIN MAGNETIC FILMS DEPOSITED IN A CONSTANT MAGNETIC FIELD

© 2024 B. A. Belyaev [a,b,*], N. M. Boev [a,c], G. V. Skomorokhov [a], P. N. Solovev [a], A. V. Lukyanenko [a,c], A. A. Gorchakovsky [a], I. V. Podshivalov [a], A. V. Izotov [a,c]

[a] *Kirensky Institute of Physics*
Siberian Branch of the Russian Academy of Sciences
660036, Krasnoyarsk, Russia
[b] *Reshetnev Siberian State University of Science and Technology*
660014, Krasnoyarsk, Russia
[c] *Siberian Federal University, 660041, Krasnoyarsk, Russia*
** e-mail: belyaev@iph.krasn.ru*

Received November 24, 2023
Revised December 29, 2023
Accepted December 29, 2023

Abstract. Strips with a length of 20 mm and width from 0.1 to 2 mm were fabricated by laser lithography from permalloy ($Fe_{20}Ni_{80}$) films with thicknesses of 50, 100, and 200 nm, obtained by magnetron sputtering on quartz substrates. In the first series of samples, the uniaxial magnetic anisotropy induced by the presence of a constant magnetic field in the film plane during deposition was oriented along the long axes of the strips, and in the second series perpendicular to them. The anisotropic properties of the samples were determined from the angular dependencies of ferromagnetic resonance fields measured on a scanning spectrometer. It was found that in the first series of samples, with decreasing strip width, the anisotropy monotonically increases several times while barely changing its direction. In the samples of the second series, it first decreases almost to zero at a certain strip width, and then rapidly grows while simultaneously rotating by $\sim 90^\circ$. The phenomenological calculation of uniaxial anisotropy in uniformly magnetized film strips shows good agreement with the experiment.

DOI: 10.31857/S004445102405e092

1. INTRODUCTION

Thin magnetic films (TMF) have been attracting researchers' attention for many years not only due to their unique properties [1-3] but also due to the possibility of creating various microwave electronic devices [4-6] and sensitive elements for weak magnetic field sensors [7-9]. It is important to note that the frequency range of such microwave devices is typically limited by the ferromagnetic resonance (FMR) frequency [10]. However, according to the Kittel equation [11], the FMR frequency for thin films with uniaxial magnetic anisotropy H_a for the case when the external field direction H coincides with the easy magnetization axis, is determined by the expression

$$\omega_0 = \gamma\sqrt{(H + H_a)(H + H_a + 4\pi M_s)},$$

where γ — is the gyromagnetic ratio, and M_s — is the saturation magnetization. Note that in general, for a selected magnetic material, the value of M_s remains practically unchanged over a wide frequency range. Consequently, the FMR frequency can be altered either by an external magnetic field or by the uniaxial anisotropy field. However, using a magnetizing system to create a magnetic field in practice leads to increased size and weight of the structure, and accordingly, to complications and higher costs of the final magnetoelectronic microwave device. Therefore, a very promising approach is to investigate the possibilities of creating magnetic films with a specified uniaxial magnetic anisotropy field for the required operating frequency range of magnetoelectronic devices. As known, there are many methods for forming uniaxial magnetic anisotropy in films. For example, it can be induced

by an external magnetic field applied in the film plane during deposition [12, 13] or after its deposition during heat treatment [14]. Magnetic anisotropy can be controlled within wide limits using the oblique deposition method [15, 16], as well as by creating elastic stresses in films made of magnetostrictive materials through various methods [17, 18].

BRecently, film structures consisting of micro- and nano-sized strips [9, 19-26], obtained by modern lithographic methods, have attracted considerable attention from researchers. Several studies have shown that in elongated microelements, there appears an additional contribution to the uniaxial magnetic anisotropy energy due to demagnetizing fields [22, 23, 25]. Studies of anisotropy behavior features depending on strip shape and distance between them have demonstrated the possibility of controlling magnetic anisotropy magnitude and, consequently, the natural FMR frequency (without constant magnetic field) in such structures within wide limits [21, 26]. However, demagnetizing fields in such microstrips are inhomogeneous, which leads to the excitation of multiple additional magnetostatic modes of magnetization oscillations [19, 20, 24], which prevent direct use of the studied structures in magnetoelectronic devices.

In this work, we investigate the anisotropic properties of local areas of individual rectangular permalloy strips with different thicknesses and different ratios of their long and short axes. Such studies allow not only to examine patterns of anisotropy behavior depending on strip width but also to demonstrate possibilities of fabricating TMF samples with predetermined magnetic anisotropy magnitude, variable within wide limits. The distinctive feature of this work is that the studied strips of specified thickness were fabricated from a single magnetic film, and their magnetic characteristics were measured using local FMR spectroscopy. This approach ensures that the observed changes in magnetic characteristics of strips of different widths are caused solely by their geometry.

2. SAMPLES AND MEASUREMENT METHODOLOGY

Magnetic films were deposited on JGS1 grade quartz glass substrates with a thickness of 0.5 mm and surface roughness less than 1 nm. The deposition was carried out using the "ORION-40 TM" system (South Korea) by magnetron sputtering of a permalloy target $Fe_{20}Ni_{80}$ manufactured by "Kurt J. Lesker" with composition purity 99.95 %. As known, such permalloy has near-zero magnetostriction, therefore almost no elastic stresses arise in the samples when magnetized in any direction. During film deposition, the argon vapor pressure in the chamber was 1.8 mbar, and the magnetron current density at the target was 21 mA/cm^2 and provided a deposition rate of 2.34 E/s. The deposition rate was determined by measuring the thickness of control films using X-ray fluorescence analysis [27], which allows determining sample thicknesses with accuracy better than ± 1 nm, and the thickness of the obtained films was calculated based on the deposition time.

To create uniaxial magnetic anisotropy in the samples, the substrates were placed in a special frame assembled from samarium-cobalt magnets in a copper casing, creating a uniform magnetic field in the film plane with magnitude $H_0 \sim 200$ Oe. This field in the substrate area is $\sim$30 times higher than the magnetron field, due to the relatively large distance from the target to the substrates$\sim$ 150 mm. It is important to note that the substrates were heated to 200°C, during deposition, which provided not only high adhesion but also minimal ferromagnetic resonance linewidth in the samples.

Studies of the influence of film shape on their anisotropic properties in the first experiment were conducted on rectangular samples with dimensions of 5×10 mm^2, deposited at the center of square substrates with dimensions of 12×12 mm^2. In each deposition cycle, two samples were simultaneously deposited through corresponding windows in the substrate holder. The long axis of one window was oriented along the constant magnetic field, while the other was perpendicular to it (Fig. 1*a*). As a result, the uniaxial magnetic anisotropy induced in the plane of the first film (*L*-sample) is oriented along its long axis, and the second (*S*-sample) along its short axis. Samples with thicknesses from 20 to 250 nm were fabricated using this method.

In the second experiment, samples deposited on substrates with dimensions of 24×30 mm^2, were studied, in two series with thicknesses of 50, 100, and 200 nm in each series. In the first series, during deposition, the long axes of the substrates, as in the first experiment, were oriented along the magnetic

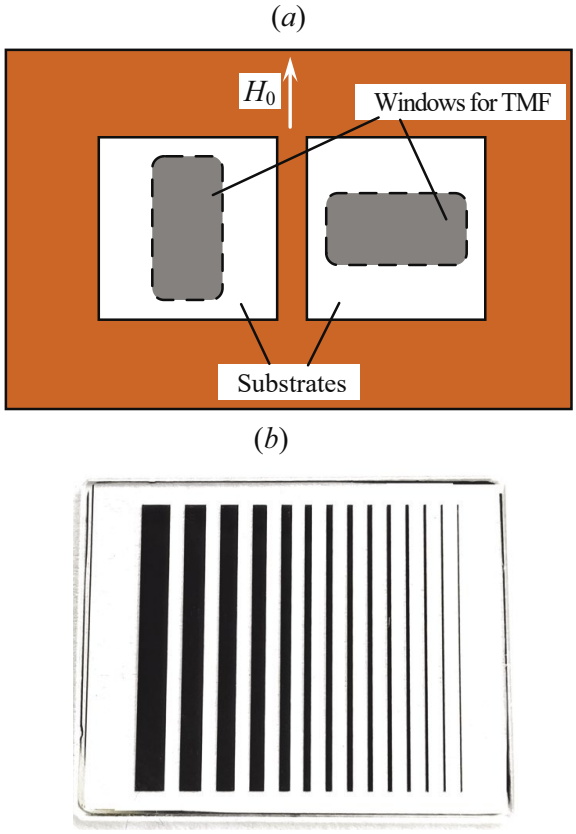

Fig. 1. Top view of the substrate holder – (*a*) and photograph of 14 TMF strips fabricated by laser lithography – (*b*)

field, and in the second series – perpendicular to it. Then, using laser lithography on a μPG 101 Heidelberg Instruments (Germany) system, 14 strips of equal length 20 mm but with decreasing width from 2.0 to 0.1 mm were fabricated by chemical etching on each film, parallel to the short side of the substrates and arranged one after another with 1 mm gaps (Fig. 1*b*). Such gaps between strips with thicknesses up to 200 nm practically exclude their interaction.

The anisotropic properties of film samples were studied using ferromagnetic resonance (FMR) method, which has high accuracy especially in the decimeter wavelength range [28]. The measurements were conducted on a scanning spectrometer [29,30] using new measuring heads [31] that significantly increase its sensitivity. The locality of measurements is determined by the hole diameter in the head of 0.8 mm, meaning the FMR signal is taken from a film area of ~ 0.5 mm^2. The planar magnetic field sweep in the spectrometer is carried out using Helmholtz coils, and the spectra were recorded on the reverse sweep to eliminate hysteresis phenomena, with the sample being magnetized by a 300 Oe field after each rotation. It is important to note that the sweep field direction in the experiments coincides with the laboratory field direction (mainly determined by Earth's field), which is automatically accounted for during spectra recording.

From the resonance field dependencies H_R, taken from the angle of the constant magnetic sweep field direction θ_H, the effective saturation magnetization M_{eff}, was determined, as well as the magnitude H_a and direction angle θ_a of the uniaxial magnetic anisotropy field of the measured film section. For this purpose, a formula was used that relates the field H_R at a fixed frequency f of the specific measuring head with the magnetic characteristics of the sample [13], excluding the negligibly small unidirectional anisotropy field in the studied samples:

$$\left(\frac{2\pi f}{\gamma}\right)^2 = [H_R\cos(\theta_H - \theta_M) + H_a\cos 2(\theta_a - \theta_M)]\times$$
$$\times [4\pi M_{eff} + H_R\cos(\theta_H - \theta_M) + H_a\cos^2(\theta_a - \theta_M)], \quad (1)$$

where the equilibrium direction θ_M of the effective saturation magnetization of the film M_{eff} is determined considering the equation

$$H_R\sin(\theta_H - \theta_M) + \frac{1}{2}H_a\sin 2(\theta_a - \theta_M) = 0, \quad (2)$$

obtained from the minimum condition of the film's free energy density [13].

To determine the parameters of magnetic films, the "FMR-extractor" program [32] was used, which allows automatic calculation of magnetic characteristics of samples from the measured dependencies $H_R(\theta_H)$, taken at the frequency f of microwave oscillations. Experiments studying the magnetic characteristics of TMF were conducted on the measuring head with a generator frequency of $f = 1.840$ GHz, at which H_R exceeds the anisotropy field during magnetic field sweep along the easy magnetization axis.

3. EXPERIMENTAL RESULTS

Figure 2 shows typical angular dependencies $H_R(\theta_H)$ of two films with dimensions 5×10 mm^2 and thickness $d = 100$ nm, measured from local areas in the center and near the edge of the samples,

marked by white dots in the figure insets. As the experiment showed, the films have different uniaxial magnetic anisotropy, as they were deposited in a planar magnetic field directed either along their long or short axes. The anisotropy field in the center of L-sample is $H_a^L = 3.8$ Oe ($\theta_a^L = 0°$), and in the center of S-sample is $H_a^S = 3.5$ Oe ($\theta_a^S = 90°$).

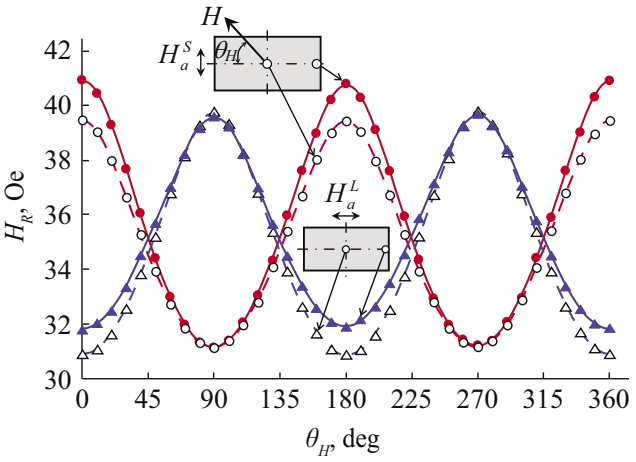

Fig. 2. Angular dependencies of FMR field for 100 nm thick films (dots – experiment, lines – calculation)

The significant difference in resonance fields between central and edge areas observed in each film, when the sweep magnetic field is oriented along the long axes of the samples, is related to demagnetizing fields arising at the film edges, which obviously lead to an increase in the resonance field H_R at these points. Considering the fact that when the sweep field is directed along the short axes of the films, the resonance fields in the center and at the edge of the samples are almost identical due to the absence of demagnetizing fields in this case, consequently, the anisotropy for S-sample at the edge point increases compared to the central point, while for L-sample it decreases.

Figure 3 shows the distributions of anisotropy field inhomogeneities (a) and effective saturation magnetization (b), measured across the area of these same samples with an equal step of 0.5 mm along coordinates x and y. It can be seen that in films of such thickness, edge effects associated with demagnetizing fields are well manifested at distances over 1 mm. Meanwhile, in the center of the films, the uniaxial magnetic anisotropy field, as already noted, is higher in L-sample than in S-sample.

Interestingly, the distributions of effective saturation magnetization across the area of both samples differ slightly from each other, and in the centers of the films, they absolutely coincide and equal $M_{eff} = 994$ emu/cm^3. It is important to note that the angles of uniaxial magnetic anisotropy direction vary very slightly across the area, and only near the film corners do they reach their maximum deviations from average values with alternating signs of these deviations at adjacent corners of the samples $\theta_a^L = 0° \pm 0.9°$, $\theta_a^S = 90° \pm 0.8°$.

Research has shown that the anisotropy field measured in the center of L-samples is always higher than in S-samples at any film thickness (Table 1). The table shows not only that the uniaxial anisotropy field $H_a^L > H_a^S$ all film thicknesses, but also that with increasing d these fields monotonically decrease, however their relative difference increases. It is also evident that the effective magnetization of films increases monotonically with increasing d. Note that the decrease in uniaxial magnetic anisotropy field and increase in M_{eff} with increasing TMF thickness was previously discovered in cobalt films [13].

Obviously, the observed relatively small difference in uniaxial magnetic anisotropy between L- and S-samples is related to the anisotropy of the rectangular shape of the films, where the long side l is only twice the length of the short side s. Therefore, it is of great interest to investigate the behavior of sample anisotropy with increasing ratio l / s. For this purpose, two series of rectangular strip samples were considered, manufactured, as previously noted, by laser lithography with 14 pieces in each series with film thicknesses of 50, 100, and 200 nm. The samples had the same length of $l = 20$ mm, but different widths s, varying from 2 to 0.1 mm (see Fig. 1*b*), for which the ratio l / s varies from 10 to 200. In the first series of samples (L-samples), the uniaxial magnetic anisotropy is directed along the TMF strips, and in the second (S-samples) – perpendicular to the strips. It is important to note that the magnetic characteristics of the samples were determined by the angular dependences of the FMR field, taken from local areas in the center of the strips. In this experiment, the samples were oriented so that at $\theta_H = 0$ the external magnetic field is directed along the width of the strips.

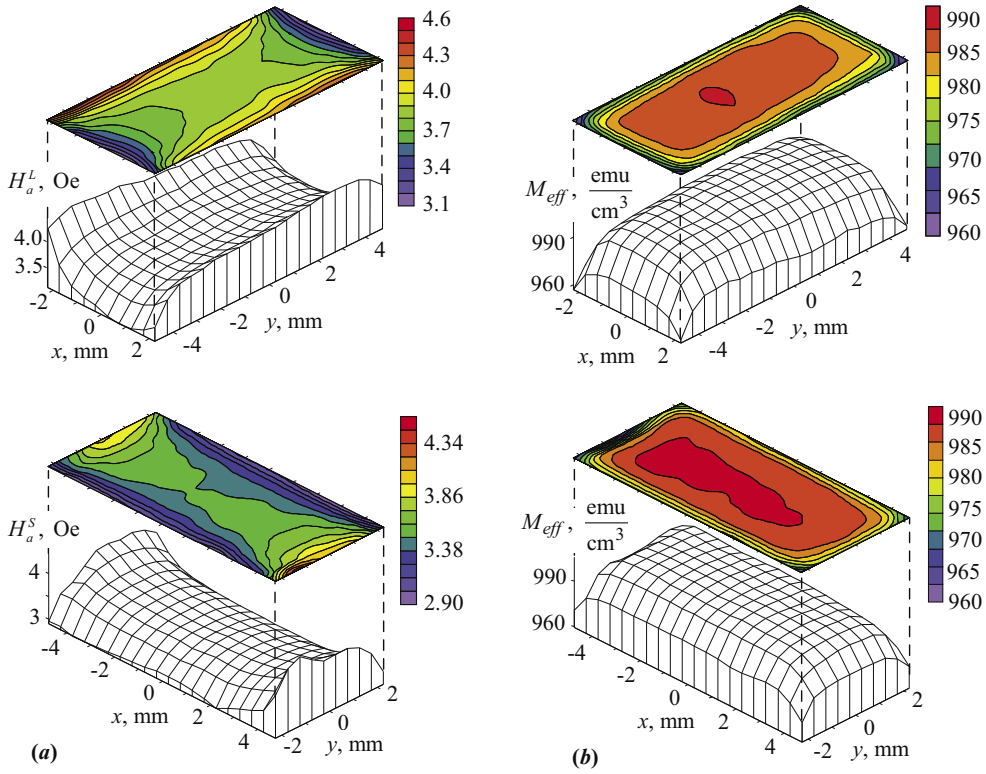

Fig. 3. Distribution of uniaxial magnetic anisotropy inhomogeneities (*a*) and effective saturation magnetization (*b*) across the area for S- and L-samples with thickness of 100 nm

Table 1. Parameters of uniaxial magnetic anisotropy, effective saturation magnetization, and relative difference of anisotropy fields in the center of films with dimensions 5 × 10 nm

d, nm	20	30	70	100	150	200	250
H_a^L / H_a^S,	5.9 / 5.8	5.2 / 5.0	4.4 / 4.1	3.8 / 3.5	3.7 / 3.0	4.0 / 3.2	3.9 / 3.1
M_{eff}, e.m.u./cm^3	913	935	979	994	1010	1110	1170
$(H_a^L - H_a^S) / H_a^L$,%	1.6	3.8	6.8	7.9	19	20	21

Figure 4 shows the dependencies $H_R(\theta_H)$, taken for L- and S-samples with film thickness $h = 100$ nm, having maximum 2 mm and minimum 0.1 mm strip width, as well as for S-sample with strip width with minimal uniaxial magnetic anisotropy $H_a^S = 0.2$ Oe. It can be seen that for L-samples, strip narrowing leads to a sharp increase in uniaxial magnetic anisotropy. For S-samples, when the strips narrow, the anisotropy first drops to almost zero at $s = 0.3$ mm, and then increases simultaneously with the rotation of the easy magnetization axis by 90°. Note that in the sample at $s = 0.3$ mm, effective cubic anisotropy (4th-order anisotropy) $H_4 = 0.3$ Oe is clearly manifested, slightly exceeding the uniaxial one.

Table 2 presents the measurement results of anisotropy fields and effective saturation magnetization in the central areas for all samples of L- and S-series with magnetic film thickness of 100 nm. It can be seen that with decreasing strip width of L-samples, the field H_a^L increases slowly at first and starting from $s < 0.75$ mm, the growth accelerates, and at $s = 0.1$ mm H_a^L exceeds the anisotropy field at $s = 2$ mm by more than 4 times. For S-samples, conversely, H_a^S first decreases to a minimum value at $s = 0.3$ mm, and then rapidly increases with simultaneous rotation of the easy magnetization axis by 90°. Meanwhile, H_a^S at $s = 0.1$ mm exceeds the anisotropy field at $s = 2$ mm by more than 2.5

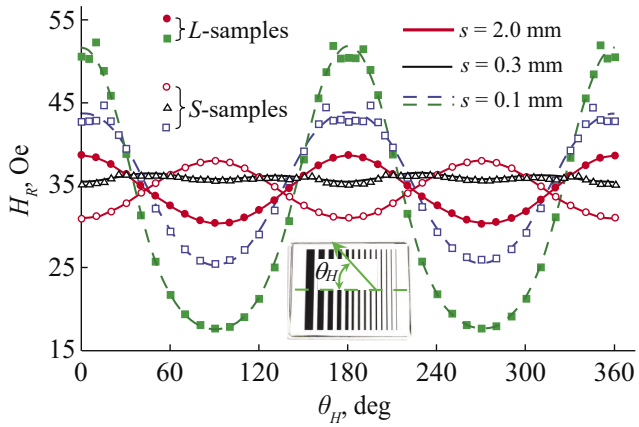

Fig. 4. Angular dependencies of FMR field for L- and S-samples from 100 nm thick films with different strip widths s (points –experiment, lines – calculation). The inset shows the orientation of the sweep field

times. The effective magnetization for each pair of films from both series is practically identical, and it monotonically decreases by only ~ 4 % with decreasing width of strip conductors.

Patterns of anisotropy fields behavior versus strip width for samples with films of different thicknesses are well observed in Fig. 5. As expected, anisotropy with decreasing strip width of L-samples almost does not change its direction at any film thickness, however, its magnitude increases, and the thicker the film, the stronger the increase.

Anisotropy of S-samples changes its direction at a certain width when strip width decreases,

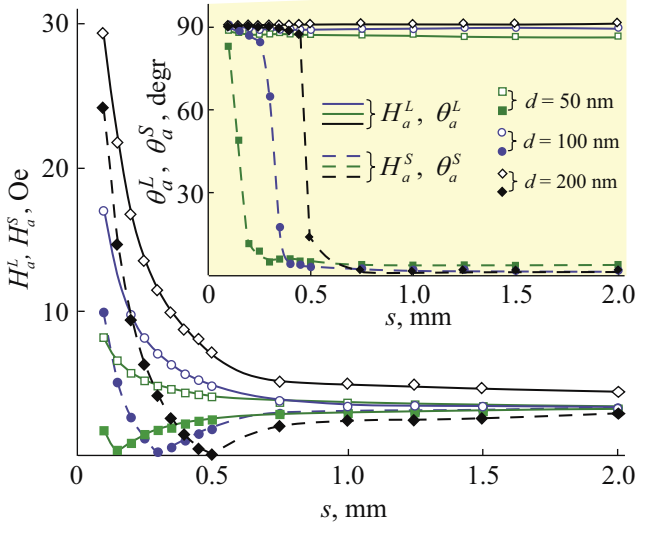

Fig. 5. Dependencies of uniaxial magnetic anisotropy parameters on strip width s for L- and S-samples with different film thicknesses d

simultaneously rotating monotonically by 90°. Meanwhile, the anisotropy magnitude of S-samples first decreases almost to zero, and then grows again. It is important to note that the minimum H_a^S for a 50 nm thick sample is observed at a strip width of 0.15 mm, for a 100 nm thick sample, as mentioned before, at a strip width of 0.30 mm, and finally, for a 200 nm thick sample at a strip width of 0.50 mm.

4. DISCUSSION OF RESEARCH RESULTS

Obviously, the results of all conducted experiments can be explained by the demagnetizing fields existing at the edges of the films. Therefore, let's calculate these fields and the associated shape anisotropy of the real thin-film sample by approximating its shape, for simplicity, as an ellipsoid. From magnetostatics, it is well known that the demagnetizing field of a magnetized ellipsoid is uniform throughout its volume, and when the ellipsoid axes coincide with the coordinate axes, this field is described by a diagonal tensor of demagnetizing coefficients with components N_x, N_y, and N_z. In general, the values of these components can only be calculated numerically. Let's consider an ellipsoid with axes $2a$, $2b$, and $2c$, lying along the coordinate axes x, y, and z respectively. For calculating the demagnetizing coefficients, it is convenient to use the expression obtained by Landau and Lifshitz [33]:

$$N_x = \frac{1}{2}\frac{b}{a}\frac{c}{a}\int_0^\infty \frac{dt}{(t+1)R(t)}, \tag{3}$$

where

$$R(t) = \sqrt{(t+1)\left(t+\frac{b^2}{a^2}\right)\left(t+\frac{c^2}{a^2}\right)}. \tag{4}$$

The formulas for demagnetizing factors along the two other directions N_y and N_z have a similar form, but with replacement in formula (3) of the term $(t+1)$ with $[t+(b/a)^2]$ for determining N_y and with $[t+(c/a)^2]$ for determining N_z.

The magnetic shape anisotropy of an ellipsoidal sample with saturation magnetization M_{eff} can be calculated using the formula xy can be calculated using the formula

$$H_d = 4\pi M_{eff}(N_x - N_y), \tag{5}$$

Table 2. Values of uniaxial magnetic anisotropy, effective saturation magnetization, and relative difference of anisotropy fields measured in the center of 100 nm thick strips versus their width

s, mm	2.0	1.5	1.25	1.0	0.75	0.5	0.45	0.4	0.35	0.3	0.25	0.2	0.15	0.1
H_a^L / H_a^S, Oe	4.1 / 3.5	4.1 / 3.3	4.3 / 3.2	4.3 / 3.2	4.4 / 3.1	5.4 / 2.1	5.7 / 1.9	6.1 / 1.4	6.7 / 0.9	7.4 / 0.2	8.3 / 0.9	9.8 / 2.3	12.1 / 4.8	17.2 / 9.2
M_{eff}, e.m.u./cm^3	990	989	988	980	966	959	958	955	953	952	951	951	952	959
$(H_a^L - H_a^S) / H_a^L$, %	15	20	26	26	30	61	67	77	87	97	89	77	60	47

where the sign will indicate the direction of the easy magnetization axis of this anisotropy, either along the axis x, or along the axis y.

The results of testing the applicability of the given formulas for calculating the parameters of the studied strips are shown in Fig. 6 for magnetic films with a thickness of 100 nm. The lines show the dependence of uniaxial anisotropy parameters on strip width, plotted according to formulas (3)-(5). In the calculations, the effective saturation magnetization for each strip was taken from Table 2, and the induced magnetic anisotropy was measured after film deposition on substrates with dimensions 24×30 mm^2 along their long axes at points where the strip centers would subsequently be located. The results of anisotropy parameter measurements at these points are shown by triangular markers in Fig. 6. Note that the induced uniaxial anisotropy values for both samples coincide at $H_a^L = 3.7$ Oe and $H_a^S = 3.7$ Oe, since the ratio of the long to short axis dimensions of the film does not exceed 1.2. The anisotropy axis angles for the L-sample are close to 90°, and for the S-sample to 0°. It is also important to note that the edge clearances for the outermost strips are more than 3.5 mm (see Fig. 1*b*), therefore edge effects do not affect the anisotropy parameter measurements.

It should be noted that for the S-sample, the calculation shows an abrupt change in the anisotropy direction at the compensation point from 0 to 90°, while in experiments (see Fig. 5 and 6), this angle changes smoothly, beginning to rotate even before the compensation point. Obviously, this is because in the calculation, the easy magnetization axis direction of the induced magnetic anisotropy coincides with the film axis ($\theta_a = 0°$), while in real samples at the measured points it is θ_a slightly larger than 0° (see Fig. 5 and 6).

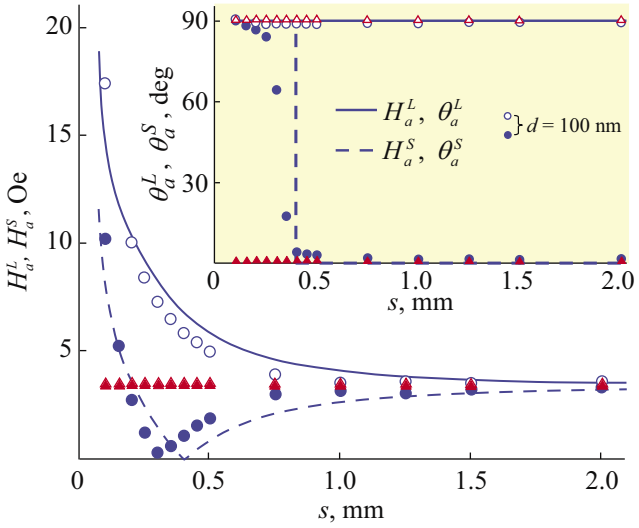

Fig. 6. Dependence of uniaxial magnetic anisotropy parameters on strip width s for L- and S-samples (points – experiment, lines – calculation). Triangular markers show the anisotropy parameters of the continuous film (before strip fabrication), measured at the same points where the strip centers would subsequently be located

The qualitative agreement between calculation results and experimental results observed in Fig. 6 proves the validity of using formulas (3)(5) to describe the shape anisotropy of the studied samples, in which, as already noted, the ratio of long to short axes varies from 10 to 200. A small difference in the compensation point of induced magnetic anisotropy during film deposition by shape anisotropy for S-sample in experiment 0.3 mm, while in theory ~0.4 mm is evidently due to the simplicity of the calculation model. Note that calculations performed for samples with film thickness of 50 and 200 nm showed the same qualitative agreement between theory and experiment. However, in these cases, the calculated compensation point for the sample with $d = 50$ nm equals ~ 0.2 mm (measured 0.15 mm), and for the sample with $d = 200$ nm

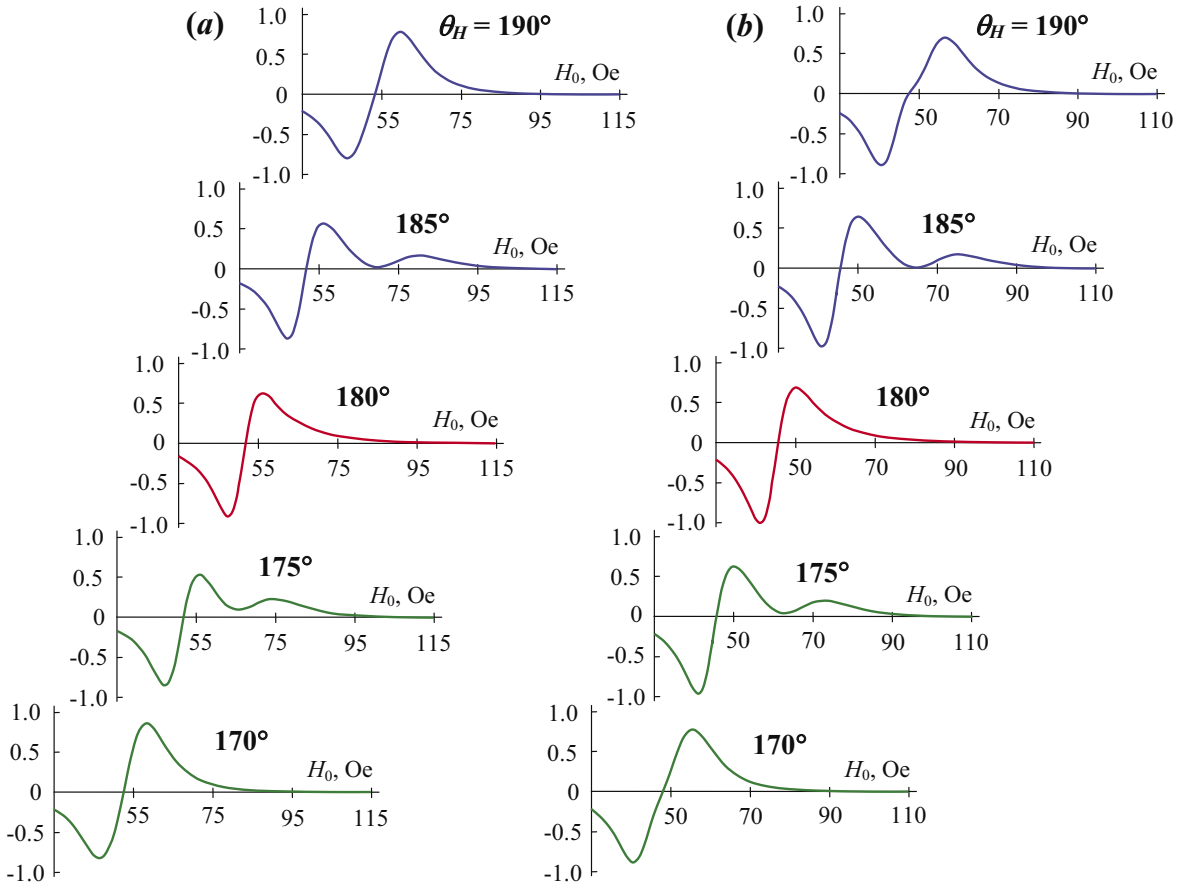

Fig. 7. FMR spectra of strips with 100 nm thickness and 0.1 mm width, recorded for several angles of sweep magnetic field direction θ_H near the hard magnetization axis, for L-sample — (*a*) and for S-sample — (*b*)

equals $\sim$ 0.7 mm (measured 0.5 mm). These facts indicate that calculations using formulas (3-5), obtained for an ellipsoidal sample shape, overestimate the demagnetizing field of the real sample, and this overestimation increases with film thickness.

The nature of the observed small "dips" in the resonance field on the angular dependencies of narrow strips near the hard magnetization axes (see Fig. 4) is associated with the excitation of some additional resonance, which reduces $H_R(\theta_H)$. The position and amplitude of this resonance strongly depend on the angle of the sweep magnetic field direction, which is clearly visible in Fig. 7. Here are presented FMR spectra taken for L- and S-samples ($d = 100$ H, $s = 0.1$ mm) at several angles θ_H. Possibly, the additional resonance is associated with the excitation of magnetostatic oscillations, which can form standing waves due to wave reflections from opposite walls, but only in narrow strips due to the relatively large damping magnitude in the studied films. For example, for a 100 nm thick film, the angleaveraged θ_H FMR linewidth measured at 1.840 GHz equals 7.06 Oe, which corresponds to the damping parameter $\alpha = 0.0093$. The proposed assumption is confirmed by experiments on an array of permalloy strips of micron length and submicron width [20, 24], in which multiple resonances of magnetostatic waves are observed.

5. CONCLUSION

It has been experimentally shown that the shape anisotropy of thin magnetic films manifests even in rectangular samples with dimensions of 5×10 mm^2 at a TMF thickness of only 20 nm. As expected, the effect increases with film thickness. These experiments gave rise to the interest to investigate the influence of anisotropy in rectangular samples of various thicknesses when changing their axis ratio over wide ranges.

As a result, the anisotropy of permalloy film samples with thicknesses of 50, 100 and 200 nm, manufactured by magnetron sputtering of a target with composition $Fe_{20}Ni_{80}$ was investigated. The films were deposited on quartz glass substrates with dimensions 24×30 mm^2, and then using laser lithography, 14 strips of equal length of 20 mm were fabricated, with decreasing width from 2 to 0.1 mm, parallel to the short side of the substrates and arranged in sequence with 1 mm gaps (Fig. 1*b*). Two series of samples were studied. In the first series, uniaxial magnetic anisotropy, induced by the presence of a constant magnetic field in the plane of the films during deposition, is oriented along the long axes of the strips (L-samples), and in the second series perpendicular to them (S-samples). The anisotropic properties of the samples were determined in local areas at the centers of the strips using angular dependencies of ferromagnetic resonance fields $H_R(\theta_H)$, measured on a scanning spectrometer.

With decreasing strip width s from 2 to 0.1 mm in the first series of samples, a monotonic increase in anisotropy by several times was observed, as the increasing shape anisotropy adds to the induced magnetic anisotropy due to the coincidence of their easy magnetization axes. Therefore, the direction of total anisotropy in the first series samples hardly changes. In the second series samples, the induced magnetic anisotropy is orthogonal to the shape anisotropy of the samples, and in samples with $s = 2$ mm it exceeds the shape anisotropy. Therefore, with decreasing s the total anisotropy first decreases almost to zero at a certain strip width, and then rapidly increases while simultaneously rotating by $\sim 90^\circ$.

To determine the parameters of uniaxial anisotropy of film strips, a phenomenological calculation was used, which considered a model of a uniformly magnetized ellipsoid. The calculation results qualitatively agree with the experiment for all L- and S-samples. A small difference between calculation and experiment in the width of strips, at which mutual compensation of induced magnetic anisotropy and shape anisotropy of S-samples is observed, is due to the simplicity of the model used in the calculation. It is shown that the phenomenological calculation for the ellipsoidal shape of the sample overestimates the demagnetizing field compared to the real sample, and this overestimation increases with increasing film thickness.

FUNDING

The work was carried out within the framework of the State Assignment scientific theme of the Kirensky Institute of Physics, Federal Research Center KSC SB RAS.

REFERENCES

1. 1. R. Suhu, Magnetic Thin Films, Mir, Moscow (1967).

2. N. M. Salansky, M. Sh. Erukhimov, Physical Properties and Applications of Magnetic Films, Nauka, Novosibirsk (1975).

3. K. Barmak, K. Coffey, Metallic Films for Electronic, Optical and Magnetic Applications: Structure, Processing and Properties, Woodhead Publ, Oxford (2014).

4. B. A. Belyaev, A. O. Afonin, A. V. Ugrymov et al., Rev. Sci. Instrum. 91, 114705 (2020).

5. A. N. Lagarkov, K. N. Rozanov, J. Magn. Magn. Mater. 321, 2082 (2009).

6. R. E. Camley, Z. Celinski, T. Fal et al., J. Magn. Magn. Mater. 321, 2048 (2009).

7. A. N. Babitsky, B. A. Belyaev, G. V. Skomorokhov et al., Tech. Phys. Lett. 41, 36 (2015).

8. A. N. Babitsky, B. A. Belyaev, N. M. Boev et al., Instrum. Exp. Tech. 3, 96 (2016).

9. G. Yu. Melnikov, I. G. Vazhenina, R. S. Iskhakov et al., Sensors 23, 6165 (2023).

10. A. N. Lagarkov, S. A. Maklakov, A. V. Osipov et al., Radio Electronics 5, 625 (2009).

11. C. Kittel, Phys. Rev. 73, 155 (1948).

12. J. Han-Min, C.-O. Kim, T.-D. Lee et al., Chinese Phys. 16, 3520 (2007).

13. B. A. Belyaev, A. V. Izotov, S. Ya. Kiparisov et al., Phys. Solid State 50, 650, (2008).

14. Y. Yang, B. Liu, D. Tang et al., J. Appl. Phys. 108, 073902 (2010).

15. P. N. Solovev, A. V. Izotov, and B. A. Belyaev, J. Magn. Magn. Mater. 429, 45 (2017).

16. Z. Ali, D. Basaula, K. F. Eid et al., Thin Solid Films 735, 138899 (2021).

17. B. A. Belyaev, A. V. Izotov, Phys. Solid State 49, 1651 (2007).

18. Z. K. Wang, E. X. Feng, Q. F. Liu et al., Physica B: Cond. Matt. 407, 3872 (2012).

19. C. Bayer, J. P. Park, H. Wang et al., Phys. Rev. B 69, 134401 (2004).

20. S. L. Vysotskii, S. A. Nikitov, Yu. A. Filimonov et al., JETP Letters 88, 534 (2008).

21. B. K. Kuanr, V. Veerakumar, L. M. Malkinski et al., IEEE Trans. Magn. 45, 3550 (2009).

22. A. Garcia-Arribas, E. Fernandez, A. V. Svalov et al., Eur. Phys. J. B 86. 136 (2013).

23. A. G. Kozlov, M. E. Stebliy, A. V. Ognev et al., IEEE Trans. Magn. 51, 2301604 (2015).

24. E. V. Skorohodov, R. V. Gorev, R. R. Yakubov et al., J. Magn. Magn. Mater. 424, 118 (2017).

25. A. G. Kozlov, M. E. Stebliy, A. V. Ognev et al., J. Magn. Magn. Mater. 422, 452 (2017).

26. Z. Zhu, H. Feng, X. Cheng et al., J. Phys. D: Appl. Phys. 51, 045004 (2018).

27. M. Haschke, J. Flock, and M. Haller, X-ray Fluorescence Spectroscopy for Laboratory Applications, Wiley-VCH, Weinheim (2021).

28. B. A. Belyaev, A. V. Izotov, JETP Letters 103, 44 (2016).

29. B. A. Belyaev, A. A. Leksikov, I. Ya. Makievskiy et al., Instruments and Experimental Techniques 3, 106 (1997).

30. B. A. Belyaev, A. V. Izotov, and A. A. Leksikov, IEEE Sensors J. 5, 260 (2005).

31. B. A. Belyaev, N. M. Boev, A. A. Gorchakovskiy et al., Instruments and Experimental Techniques 2, 107 (2021).

32. A. V. Izotov, B. A. Belyaev, Computer Program State Registration Certificate No. 2009616881 (2009).

33. L. D. Landau, E. M. Lifshitz, Electrodynamics of Continuous Media, Nauka, Moscow (1982).